J. Fluid Mech. (2002), *vol.* 458, *pp.* 181–190.
DOI: 10.1017/S0022112002007991 Printed in the United Kingdom

A low-dimensional model for simulating three-dimensional cylinder flow

By XIA MA AND GEORGE EM KARNIADAKIS

Division of Applied Mathematics, Brown University, Providence, RI 02912, USA

(Received 19 November 2001 and in revised form 17 January 2002)

We investigate the stability and dynamics of three-dimensional limit-cycle states in flow past a circular cylinder using low-dimensional modelling. High-resolution direct numerical simulations are employed to obtain flow snapshots from which the most energetic modes are extracted using proper orthogonal decomposition. We show that the limit cycle is reproduced very accurately with only twenty three-dimensional modes. The addition of two-dimensional modes to the Karhunen–Loeve expansion basis improves the ability of the model to capture the three-dimensional bifurcation, including the discontinuity in the Strouhal number discovered experimentally.

1. Introduction

In this paper we construct a low-order dynamical system to simulate the three-dimensional flow past a circular cylinder. From the practical point of view, such models are useful for control applications, e.g. Balasubramanian *et al.* (2001). From the theoretical point of view, it is interesting to investigate the existence and the accuracy of such low-dimensional representations. The feasibility for flow model reduction can be proved rigorously only for a few simple flows, see Robinson (2001), but experimental and numerical evidence suggests that many complex flows exhibit low-dimensionality and can potentially be described by approximate inertial manifolds, see Deane *et al.* (1991), Cao & Aubry (1993), Ma, Karamanos & Karniadakis (2000) and references therein for the cylinder flow. Several different approaches to reduced modelling have been proposed for the cylinder flow, mainly in investigating the first Hopf bifurcation but also covering other aspects, e.g. Sreenivasan, Strykowski & Olinger (1987), Leweke & Provansal (1994), Albarede & Provansal (1995), Olinger (1993). Here we are interested in the three-dimensional flow states, which are slightly above the secondary instability. This regime was first modelled by Noack & Eckelman (1994) using a low-order spectral Galerkin system. A review of the physical mechanisms in this range of Reynolds number was provided by Williamson (1996); see also references therein.

In the numerical work of Noack & Eckelman (1994) a spectral tensor basis was adopted, scaled appropriately with the boundary layer to reflect the Reynolds number effect, and 189 modes were employed in their simulations. Although hierarchical (in the index space) such modes are not directly related to the flow energetics. Our objective is different: we aim to construct low-dimensional systems which are based on the hierarchical most energetic flow scales with an order of magnitude reduction in the required modes, i.e. based on ten to twenty modes. The approach followed in

Deane *et al.* (1991) and Cao & Aubry (1993) for the two-dimensional cylinder flow was based on empirical eigenfunctions derived by proper orthogonal decomposition (POD). We will adopt the same procedure in the current work.

Proper orthogonal decomposition is a methodology that first identifies the most energetic modes in an evolving system, and second provides a means of obtaining a low-dimensional description of the system's dynamics. Background material for the POD approach can be found in the review article by Bekooz, Holmes & Lumley (1993). Here we adopt the implementation based on the *method of snapshots* developed by Sirovich (1987). POD has been used so far in conjunction with experimental (e.g. Glezer, Kadioglu & Pearlstein 1989; Citriniti & George 2000; Arndt, Long & Glauser 1997; Gordeyev & Thomas 2000; Delville *et al.* 1999) and numerical studies (e.g. Deane *et al.* 1991; Sirovich 1987; Aubry *et al.* 1988; Rempfer & Fasel 1994; Liakopoulos, Blythe & Gunes 1997).

We have employed spectral direct numerical simulation (DNS) to obtain detailed snapshots of the flow for Reynolds number (based on cylinder diameter and free-stream velocity) 150 to 200. The eigenmodes obtained are truly three-dimensional, i.e. we have not assumed a Cartesian tensor-like decomposition along the homogeneous spanwise direction. The dynamical systems are constructed based on a varying number of these eigenmodes, from $M = 6$ to 40 as will be discussed in the next section, using linear Galerkin projections. In addition, appropriate hybrid trial bases were sought that accommodate the reverse transition, i.e. from the three-dimensional to two-dimensional states.

2. Formulation of dynamical systems

2.1. *Eigenspectrum and POD modes*

The original data required for the construction of dynamical systems were obtained by DNS based on spectral/hp element discretizations. The method and its validation for cylinder flow for Reynolds number Re up to 5000 is described in Ma *et al.* (2000). For the current simulations we used the smaller mesh consisting of 412 triangular elements of spectral order seven, with eight Fourier collocation points along the span. The length of the cylinder span was $L_z/d = 4$, where d is the cylinder diameter; it was based on the critical length obtained in the Floquet analysis of Barkley & Henderson (1996). We investigate the range $Re = 180 \pm 20$ as we target the three-dimensional limit cycle, the onset of which was obtained in Barkley & Henderson (1996) to be at $Re_c = 188.5 \pm 1.0$. In the current simulations, we obtain the first limit cycle with non-negligible spanwise velocity component at a slightly lower value, $Re \approx 185$, which is closer to the experiments of Williamson (1989), Hammache & Gharib (1991) and Zhang *et al.* (1995). Specifically, both simulations and experiments reported in Zhang *et al.* (1995) and the Floquet analysis of Noack & Eckelman (1994) show a critical Reynolds number for the secondary instability around 170.

In order to obtain the most energetic eigenmodes from the DNS databases we need to construct the *covariance matrix* of the velocity vector field correlating all points in the domain. Assuming that the total number of points in space is n, then the covariance matrix is $n \times n$. For the three-dimensional simulations employed here $n \approx 300\,000$ and thus it is impractical to work with such a big eigensystem. To this end, we employ the snapshot method of Sirovich (1987), which we formulate as follows:

Let $\boldsymbol{V}(\boldsymbol{x}, t)$ be a time-dependent velocity field and $\boldsymbol{U}(\boldsymbol{x})$ its average, then we

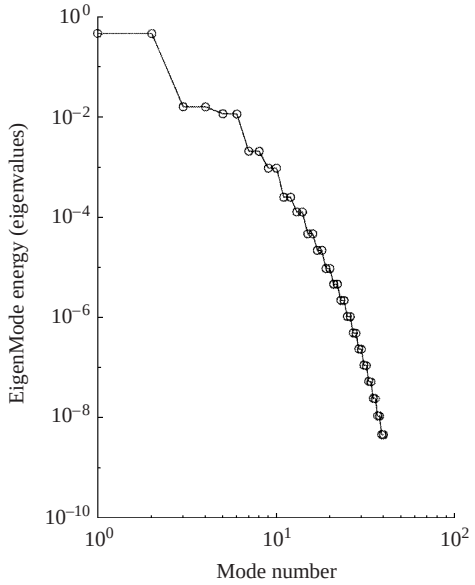

FIGURE 1. Normalized eigenvalues for three-dimensional flow past a cylinder at $Re = 185$.

decompose $\boldsymbol{V}$ as

$$\boldsymbol{V}(\boldsymbol{x}, t) = \boldsymbol{U}(\boldsymbol{x}) + \boldsymbol{u}(\boldsymbol{x}, t),$$

where $\boldsymbol{u}$ defines the perturbation velocity, which is represented by the Karhunen–Loeve expansion

$$\boldsymbol{u}(\boldsymbol{x}, t) = \sum_{m=1}^{M} \boldsymbol{\phi}_m(\boldsymbol{x}) a_m(t),$$

where $\boldsymbol{\phi}_m(\boldsymbol{x})$ is the trial basis and $a_m(t)$ the time-dependent coefficients. In the snapshot method, a_m is the eigenfunction of the covariance matrix

$$C_{p,q} = \int_{\Omega} \boldsymbol{u}(\boldsymbol{x}, t_p) \cdot \boldsymbol{u}(\boldsymbol{x}, t_q)\, \mathrm{d}\boldsymbol{x},$$

where

$$\boldsymbol{u} = u(x, y, z)\boldsymbol{i} + v(x, y, z)\boldsymbol{j} + w(x, y, z)\boldsymbol{k}.$$

The POD *vector* mode $\boldsymbol{\phi}(\boldsymbol{x})$ is defined by

$$\boldsymbol{\phi}(\boldsymbol{x})_m = \int a_m(t)\boldsymbol{u}(\boldsymbol{x}, t)\, \mathrm{d}t. \tag{2.1}$$

The above was put in matrix form and the eigenspectrum and corresponding eigenmodes were obtained using standard LAPACK routines. The normalized POD modes obtained are 'numerically' orthogonal, as they are perpendicular to each other within at least 10^{-8} accuracy for the higher modes and 10^{-14} on the average, see Ma (2001).

The eigenspectrum computed at $Re = 185$ based on 40 snapshots is shown in figure 1. The modes form pairs due to the closeness of the vortex street to a travelling wave, similarly to the two-dimensional flow studied in Deane *et al.* (1991). This is also reflected in the eigenmodes of each pair, which are phase-shifted with respect to each other. A qualitative picture of the structure of the POD modes is provided in figure 2 that presents the first, third, tenth and twentieth modes of the

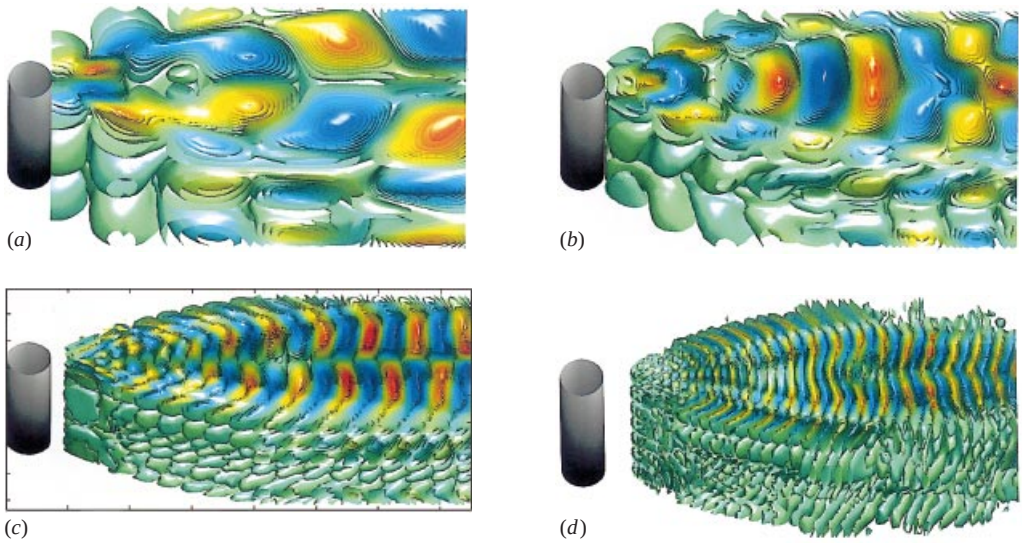

FIGURE 2. Contours of the w velocity component for mode (a) first; (b) third; (c) tenth, and (d) twentieth. $Re = 185$.

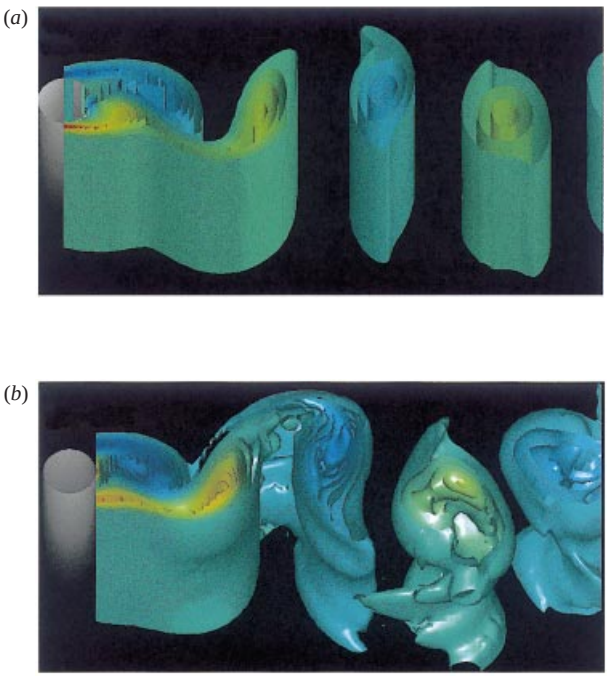

FIGURE 8. POD simulations (system B). Spanwise vorticity Ω_z at $Re = 183$ (a), and at $Re = 185$ (b).

spanwise velocity component w. These are three-dimensional, geometry-fitted global eigenmodes, for which, unlike tensor-product expansions, it is not exactly predictable how scale information is introduced, e.g. which Cartesian direction is refined as the mode index increases. Similar patterns were obtained for the streamwise and cross-flow components, see Ma (2001). Finally, we note that based on the energy decay

shown in the eigenspectrum plot, it appears that at least the first six modes are energetically significant and should be retained in the truncation of the system.

2.2. *Galerkin projection*

The dynamical systems are obtained by performing a Galerkin projection of the incompressible Navier–Stokes equations onto the space spanned by the POD modes, i.e.

$$\int_\Omega \boldsymbol{\phi}_m(\boldsymbol{x}) \cdot \left(\frac{\partial \boldsymbol{V}}{\partial t} + (\boldsymbol{V} \cdot \nabla)\boldsymbol{V} + \nabla p - \frac{1}{Re}\nabla^2 \boldsymbol{V} \right) \mathrm{d}\boldsymbol{x} = 0, \tag{2.2}$$

$$\int_\Omega \boldsymbol{\phi}_m(\boldsymbol{x}) \cdot (\nabla \cdot \boldsymbol{V})\, \mathrm{d}\boldsymbol{x} = 0. \tag{2.3}$$

The divergence-free equation (2.3) is satisfied automatically since the POD modes are divergence-free by construction, i.e.

$$\nabla \cdot \boldsymbol{\phi}_m(\boldsymbol{x}) = \nabla \cdot \int a_m(t)\boldsymbol{u}(\boldsymbol{x})\, \mathrm{d}t = \int a_m(t) \nabla \cdot \boldsymbol{u}\, \mathrm{d}t = 0,$$

where both the average field and fluctuations are also divergence-free.

Based on this, the pressure term drops out from the governing equations since

$$\int_\Omega \boldsymbol{\phi}_m(\boldsymbol{x}) \cdot \nabla p \ \mathrm{d}\boldsymbol{x} = \int_\Gamma p\ \boldsymbol{\phi} \cdot \boldsymbol{n} \ \mathrm{d}\boldsymbol{x} - \int_\Omega (\nabla \cdot \boldsymbol{\phi}_m) p \ \mathrm{d}\boldsymbol{x} = 0,$$

where at the boundary Γ, we have imposed either $p = 0$ at the outflow, periodicity at the side boundaries, and $\phi = 0$ on the cylinder surface and inflow. More details can be found in Deane *et al.* (1991) and Ma (2001).

3. Stability of low-dimensional models

The two-dimensional cylinder flow was studied in Dean *et al.* (1991); it was found that six POD modes are sufficient to reproduce the flow dynamics, which was stable for about 100 shedding cycles. Having obtained the three-dimensional modes we have considered a similar problem for the three-dimensional flow targeting the first (harmonic) limit cycle. In particular, we compared systematically two low-dimensional systems: the first (system A) is constructed based on 40 POD modes at $Re = 185$; the second (system B) is constructed by combining 20 modes extracted at $Re = 185$ and 20 modes extracted at a subcritical Reynolds number $Re = 182$. This hybrid system can be constructed either by concatenating the two sets of snapshots at the corresponding Reynolds number or by extracting the POD modes at each state and subsequently orthonormalizing the entire set.

We have obtained low-dimensional models for $M = 6, 10, 20$ and 40 modes for both systems A and B. The results with $M = 20$ for the system A are shown in figures 3 and 4 and correspond to $Re = 185$. A stable limit cycle is obtained for at least 500 convective times units (here plotted for 200 units), which corresponds to about 100 shedding cycles. The corresponding phase portraits, constructed by cross-plotting the coefficients of high modes versus the first mode, are in excellent agreement with the corresponding DNS data projected onto the 20 modes used in the low-dimensional model. The simulation with $M = 40$ modes is almost indistinguishable from the simulation with $M = 20$ modes for the first 15 modes. However, for higher modes there is a noticeable difference as shown in figure 5, where the time history of the twentieth mode is compared for the two truncations and also versus the DNS data.

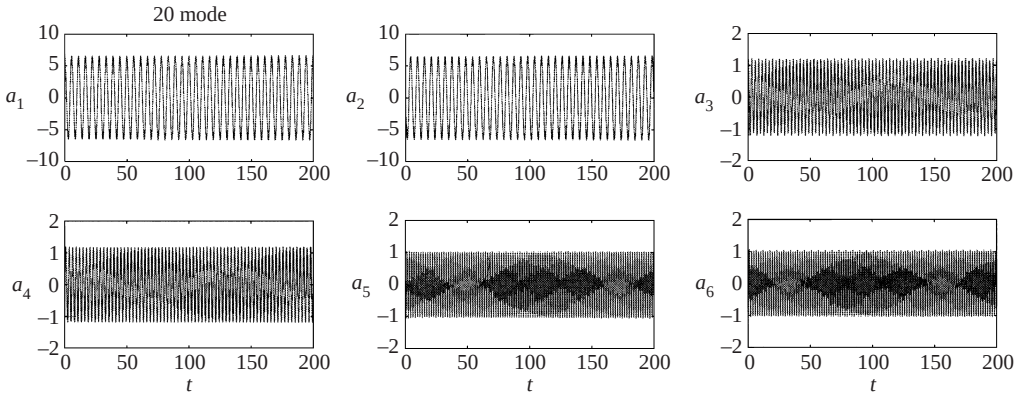

FIGURE 3. Variation of coefficients of different modes with time for system A. $M = 20$ and $Re = 185$.

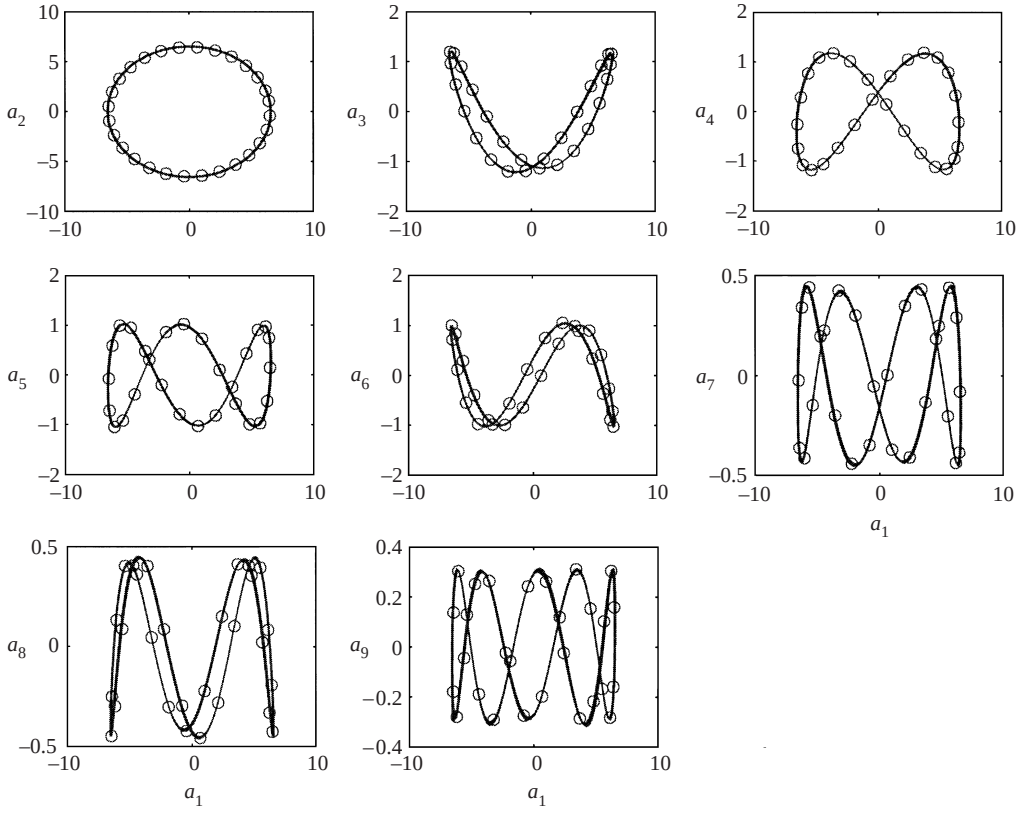

FIGURE 4. Phase portraits of coefficients corresponding to higher modes versus the first mode for system A. The last 35 shedding periods are plotted. The circles correspond to DNS data and the lines to POD predictions. $M = 20$ and $Re = 185$.

Comparing system A with system B in figure 5 we observe that the expansion with 40 modes is almost identical; however, there are noticeable differences in the expansion with 20 modes. Finally, the simulations with $M = 6$ and 10 converge to states with smaller and larger amplitude, respectively, for the two truncations compared

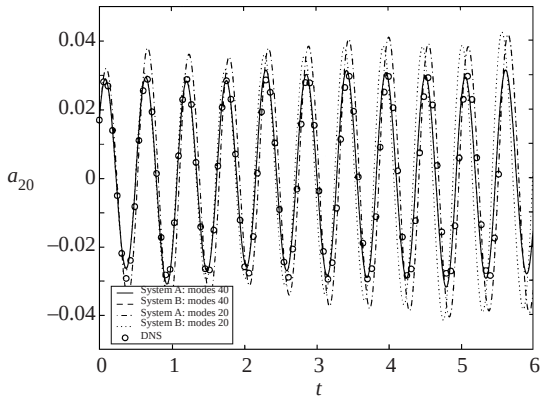

FIGURE 5. Comparison of the time history of the 20th mode of systems A and B for truncations with 20 and 40 POD modes.

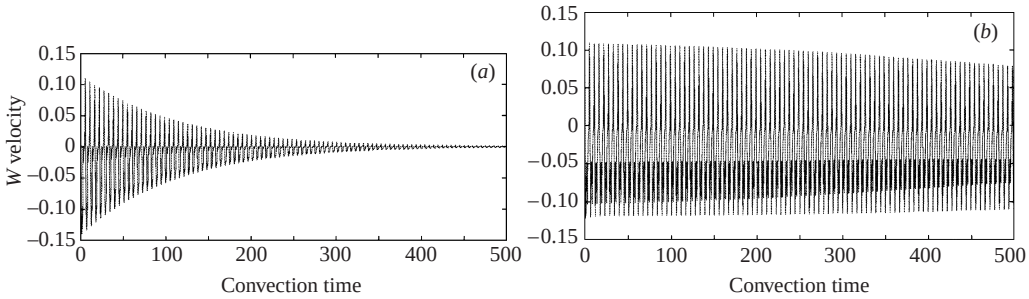

FIGURE 6. Time history of spanwise velocity w at $x/d = 2.55, y = -0.45$, showing the convergence trend at the subcritical $Re = 183$ for (a) system B (hybrid), and (b) system A.

to the DNS data. These new states exhibit about 10% differences from the DNS data.

The hybrid system B exhibits similar behaviour as system A, i.e. it is stable and converges to the correct limit cycle at $Re = 185$. In addition, it predicts correctly the transition from the three-dimensional to a two-dimensional state as shown in figure 6(a). In contrast, system A shows a very slow decaying of the spanwise velocity component, plotted in figure 6(b). In fact, even at lower Reynolds number, e.g. $Re = 170$, POD simulations based on system A show a very long transient and a residual (finite) spanwise velocity even after a very long time integration (about 2000 shedding cycles). Another major difference between systems A and B is that the latter predicts correctly the jump in the Strouhal number versus Reynolds number curve in agreement with the experiments of Williamson (1988) and Hammache & Gharib (1991). This is shown in figure 7, where the experimental results are also presented. Specifically, the Strouhal peak predicted by POD (system B) is $St = 0.183$ at $Re = 185$ and $St = 0.194$ at $Re = 183$. This transition manifests also itself in the flow structure of the near wake as spanwise modulation. Figure 8 shows iso-surfaces of spanwise vorticity (Ω_z); panel (a) corresponds to $Re = 183$, and (b) to $Re = 185$. The results are based on POD simulation with system B composed of 40 hybrid modes.

Finally, at higher Reynolds number, systems A and B diverge. For example, POD simulations at $Re = 189$ show a stable limit cycle for short time integration (about five shedding cycles), but they diverge for the long time integration.

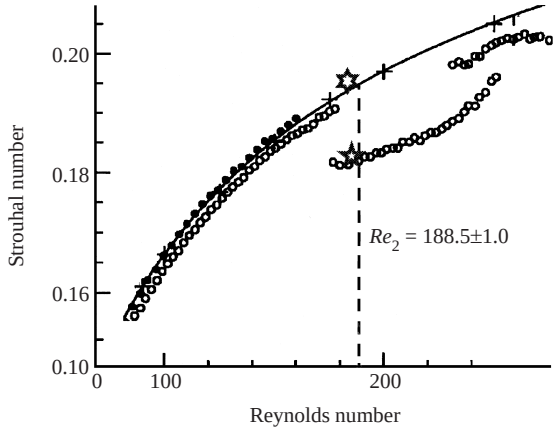

FIGURE 7. Strouhal number versus Reynolds number. ○, experiments of Williamson (1988); ●, experiments of Hammache & Gharib (1991); + (line), two-dimensional simulations of Barkley & Henderson (1996); ⋆, current POD simulations. The vertical lines denote transitions obtained in Barkley & Henderson (1996).

4. Discussion

We have simulated the three-dimensional limit cycle state in uniform flow past a circular cylinder at $Re = 185$ using a low-dimensional Galerkin model. The trial basis was constructed based on hierarchical modes extracted from DNS databases following a POD procedure. Particular attention was paid on the construction of a Karhunen–Loeve expansion that captures accurately both the limit cycle and the transition to three-dimensionality. To this end, we demonstrated that a *hybrid basis* consisting of both three- and two-dimensional POD modes representing nearby states is the proper choice.

Unlike previous work in POD modelling, we did not incorporate any *ad hoc* eddy viscosity models in order to stabilize the computations. The Galerkin models we constructed based on 20 or more modes were sufficiently dissipative to result in stable long-term dynamics that lasts a few hundred shedding cycles. This may be sufficient from the practical point of view, e.g. in control applications. However, the question remains if such severe truncations of the dynamical system are asymptotically stable, i.e. for all times. The answer is not clear. We have seen, for example, for the flow we studied here that after a long time a small divergence appears that eventually renders the system unstable. If more modes are included the onset of divergence is delayed but the same picture emerges.

We have also observed such long-term divergence for the two-dimensional flow, where systematic studies are more affordable. However, in both cases a selective filering based on the spectral vanishing viscosity method, see Karamanos & Karniadakis (2000), stabilizes the simulation (consistent with the observation of Rempfer (1993) that the 'turbulent viscosities' of the POD modes increase with their index). We have also found that if a cylinder is inside a channel (internal flow) the long-term flow dynamics is stable at all times without explicit filtering. Similarly, if the circular cylinder flow is forced slightly, say with some small inflow oscillating component, the corresponding dynamical system is stable without the incorporation of eddy viscosity. Finally, another approach that has been effective in obtaining stable low-dimensional systems, even for severe truncations, is based on *nonlinear Galerkin projections*, see Jauberteau, Rosier & Temam (1997) and Ma (2001). The high modes are 'enslaved'

into the lower more energetic modes and provide sufficient dissipation for stable long-term dynamics. We are still investigating these open issues and will report our progress in a future publication.

This work was supported partially by ONR, NSF and DOE. The computations were performed on the IBM SP3 at Maui High Performance Computing Center (MHPCC), at the NCSA University of Illinois (Urbana-Champaign) and at the Center for Scientific Computing & Visualization at Brown University.

REFERENCES

Albarede, P. & Provansal, M. 1995 Quasi-periodic cylinder wakes and the Ginzburg–Landau model. *J. Fluid Mech.* **291**, 191–222.

Arndt, R., Long, D. & Glauser, M. 1997 The proper orthogonal decomposition of pressure fluctuations surrounding a turbulent jet. *J. Fluid Mech.* **340**, 1–33.

Aubry, N., Holmes, P., Stone, J. & Lumley, J. 1988 The dynamics of coherent structures in the wall region of a turbulent boundary layer. *J. Fluid Mech.* **192**, 115–173.

Balasubramanian, G., Olinger, D., Demetriou, M. & Davis, M. 2001 Development of a self-learning coupled map lattice scheme for modeling cylinder wakes. *J. Fluids Struct.* (submitted).

Barkley, D. & Henderson, R. 1996 Three-dimensional Floquet stability analysis of the wake of a circular cylinder. *J. Fluid Mech.* **322**, 215–241.

Bekooz, G., Holmes, P. & Lumley, J. 1993 The proper orthogonal decomposition in the analysis of turbulent flows. *Annu. Rev. Fluid Mech.* **25**, 539–575.

Cao, N.-Z. & Aubry, N. 1993 Numerical simulation of wake flow via a reduced system. *Proc. ASME Fluids Engineering Conference, Washington DC*.

Citriniti, J. & George, W. 2000 Reconstruction of the global velocity field in the axisymmetric mixing layer utilizing the proper orthogonal decomposition. *J. Fluid Mech.* **418**, 137–166.

Deane, A., Kevrekidis, I., Karniadakis, G. & Orszag, S. 1991 Low-dimensional models for complex geometry flows: application to grooved channels and circular cylinders. *Phys. Fluids* A **3**, 2337–2354.

Delville, J., Ukeiley, L., Cordier, L., Bonnet, J. & Glauser, M. 1999 Examination of large-scale structures in a turbulent plane mixing layer. Part 1. Proper orthogonal decomposition. *J. Fluid Mech.* **391**, 91–122.

Glezer, A., Kadioglu, Z. & Pearlstein, A. 1989 Development of an extended proper orthogonal decomposition and its application to a time periodically forced plane mixing layer. *Phys. Fluids* A **1**, 1363.

Gordeyev, S. & Thomas, F. 2000 Coherent structure in the turbulent planar jet. Part 1. Extraction of proper orthogonal decomposition eigenmodes and their self-similarity. *J. Fluid Mech.* **414**, 145–194.

Hammache, M. & Gharib, M. 1991 An experimental study of the parallel and oblique vortex shedding from circular cylinders. *J. Fluid Mech.* **232**, 567–590.

Jauberteau, F., Rosier, C. & Temam, R. 1997 A nonlinear Galerkin method for the Navier–Stokes equations. *Comput. Meth. Appl. Mech. Engng* **8**, 245–260.

Karamanos, G. & Karniadakis, G. 2000 A spectral vanishing viscosity method for large-eddy simulations. *J. Comput. Phys.* **162**, 22–50.

Leweke, T. & Provansal, M. 1994 Model for the transition in bluff-body wakes. *Phys. Rev. Lett.* **72**, 3147–3177.

Liakopoulos, A., Blythe, P. & Gunes, H. 1977 A reduced dynamical model of convective flows in tall laterally heated cavities. *Proc. R. Soc. Lond.* A **453**, 663–672.

Ma, X. 2001 Hierarchical Galerkin and non-linear Galerkin models for laminar and turbulent wakes. PhD thesis, Division of Applied Mathematics, Brown University.

Ma, X., Karamanos, G. & Karniadakis, G. 2000 Dynamics and low-dimensionality of the turbulent near-wake. *J. Fluid Mech.* **410**, 29–65.

Noack, B. & Eckelman, H. 1994 A low-dimensional Galerkin method for the three-dimensional flow around a circular cylinder. *Phys. Fluids* **6**, 124–143.

Olinger, D. 1993 A low-dimensional model for chaos in open fluid flows. *Phys. Fluids* **5**, 1947.

Rempfer, D. 1993 Low-dimensional models of a flat-plate boundary layer. In *Proceedings of Near-Wall Turbulent Flows* (ed. R. M. C. So, C. G. Speziale & B. E. Launder), pp. 63–72. Elsevier.

Rempfer, D. & Fasel, H. 1994 Evolution of three-dimensional coherent structures in a flat-plate boundary layer. *J. Fluid Mech.* **260**, 351–375.

Robinson, J. 2001 A rigorous treatment of 'experimental' observations for the two-dimensional Navier–Stokes equations. *Proc. R. Soc. Lond.* A **457**, 1007–1020.

Sirovich, L. 1987 Turbulence and the dynamics of coherent structures, Parts I, II and III. *Q. Appl. Maths* **XLV**, 561–590.

Sreenivasan, K., Strykowski, P. & Olinger, D. 1987 Hopf bifurcation, Landau equation, and vortex shedding behind circular cylinders. In *ASME Forum on Unsteady Flow Separation*, vol. 52 (ed. R. M. C. So, C. G. Speziale & B. E. Launder), pp. 63–72. Elsevier.

Williamson, C. 1988 The existence of two stages in the transition to three-dimensionality of a cylinder wake. *Phys. Fluids* **31**, 3165–3168.

Williamson, C. 1989 Oblique and parallel modes of vortex shedding in the wake of a circular cylinder at low Reynolds numbers. *J. Fluid Mech.* **206**, 579–627.

Williamson, C. 1996 Vortex dynamics in the cylinder wake. *Annu. Rev. Fluid Mech.* **28**, 477–539.

Zhang, H., Fey, U., Noack, B., Konig, M. & Eckelman, H. 1995 On the transition of the cylinder wake. *Phys. Fluids* **7**, 779–794.